# Semi-Supervised Fuzzy DBN-Based Broad Learning System for Forecasting ICU Admissions in Post-Transplant COVID-19 Patients

Xiao Zhang and Àngela Nebot
*Soft Computing Research Group at the Intelligent Data Science and Artificial Intelligence Research Center, Universitat Politècnica de Catalunya, Barcelona, Spain*

Keywords: Fuzzy System, Broad Learning System, ICU, Covid-19, Manifold Regularization, Organ Transplant.

Abstract: This paper introduces a novel semi-supervised neuro-fuzzy system to predict ICU admissions among post-COVID organ transplant recipients. Addressing the challenges of small sample sizes and lacking labels in organ transplantation, our study takes on these issues by proposing a DBN-Based Dual Manifold Regularized Fuzzy Broad Learning System (D-DMR-FBLS). This system utilizes the streamlined and flat architecture of the Broad Learning System (BLS), integrating Deep Belief Networks (DBN) and Takagi-Sugeno-Kang (TSK) systems to enhance representation learning capacities during the Unsupervised Training Phase (UTP). The system combines the strong feature learning capabilities of DBN with the powerful fuzzy rule extraction capacity of the TSK system, enhancing the model's predictive performance and generalization capability. Moreover, we propose two types of graph-based manifold regularization, sample-based and feature-based, within this novel D-DMR-FBLS framework. Our method enhances its predictive ability by exploiting both the similarity among unlabeled and labeled patient samples, as well as the correlations between features within the fuzzy feature space. Employed to predict ICU admission risks in post-transplant COVID-19 patients, the method has demonstrated superior performance over existing methods, particularly in scenarios with limited samples and labels, thereby providing more accurate decision support for medical professionals in optimizing resource allocation for transplant patients.



## 1 INTRODUCTION

Since its emergence in late 2019, COVID-19 has led to over 700 million infections and caused more than 6 million deaths globally, constituting a major public health crisis (Worldometer, 2024). Organ transplant recipients, particularly vulnerable due to their compromised immune systems and reliance on immunosuppressants, have faced increased mortality risks during this period (Mamode et al., 2021). The pandemic has intensified the demand for critical medical resources such as ventilators and ICU beds, highlighting the urgent need for better medical oversight and protection for these at-risk patients. Current research on optimizing medical resource allocation for transplant recipients using machine learning (ML) is insufficient. Utilizing ML to predict the medical needs of these patients can identify those at highest risk more effectively, thereby optimizing resource allocation, reducing the load on healthcare systems, and potentially decreasing mortality rates in this group. Moreover, precise predictive models can assist in clinical decision-making and play a vital role in managing resource distribution during peak demand periods, ensuring that critical support is directed towards those most in need.

Current research in organ transplantation increasingly utilizes machine learning (ML) to predict post-transplant survival rates, with Random Forest (RF), XGBoost and deep learning (DL) gaining popularity for their accuracy and ease of implementation, as noted in recent studies (Liu et al., 2020; Mark et al., 2023). However, the efficacy of advanced DL models, does not consistently outperform ensemble learning models in this domain, often showing limited performance improvements despite increased complexity, particularly with data granularity challenges (Zhang et al., 2022; Ershoff et al., 2020). In contrast, Fuzzy Neural Networks (FNN) are recognized for their ability to manage non-linearity and high-dimensional data effectively, crucial for handling the inherent uncertainty and ambiguity in complex medical datasets (Shihabudheen and Pillai, 2018).



Zhang, X. and Nebot, À.
Semi-Supervised Fuzzy DBN-Based Broad Learning System for Forecasting ICU Admissions in Post-Transplant COVID-19 Patients.
DOI: 10.5220/0012856300003758

In *Proceedings of the 14th International Conference on Simulation and Modeling Methodologies, Technologies and Applications (SIMULTECH 2024)*, pages 415-422
ISBN: 978-989-758-708-5; ISSN: 2184-2841

The Fuzzy Broad Learning System (FBLS) represents an innovative integration of fuzzy logic into the Broad Learning System (BLS), creating a framework particularly adept at handling ambiguous or imprecise data (Feng and Chen, 2018; Feng and Chen, 2021; Feng et al., 2020; Liu et al., 2021; Gong et al., 2021; Zhang et al., 2020). FBLS leverages the advantage of fuzzy logic to enhance its capability to process uncertain information, thereby increasing its efficiency in environments characterized by data ambiguity. A distinctive feature of FBLS is its streamlined, flat network architecture derived from BLS. This architecture facilitates rapid feature learning and expedites information processing, setting it apart from hierarchical deep learning models. Such a configuration makes FBLS particularly well-suited for managing high-dimensional and nonlinear data sets.

The transplantation field faces the challenge of a scarcity of labeled samples, stemming from privacy concerns and the frequent loss of follow-up among recipients. This limitation complicates the collection of adequate labeled data essential for traditional supervised learning models. Addressing the challenges of small sample sizes and lacking labels in the organ transplantation domain, this paper presents a novel neuro-fuzzy system named the DBN-based Dual-Manifold Regularized Fuzzy Broad Learning System (D-DMR-FBLS). In the unsupervised training phase, DBN (Deep Belief Networks) and TSK (Takagi-Sugeno-Kang) fuzzy systems are integrated for representation learning. This system leverages the strengths of DBN in deep feature extraction and representational learning, along with the flexibility of TSK fuzzy systems in handling uncertainty and fuzzy information. Furthermore, this system also incorporates two types of graph-based manifold regularization strategies: feature manifold regularization and sample manifold regularization. Sample manifold regularization exploits the geometric distribution of samples to enhance the model's capability to capture and utilize the intrinsic associations and similarities among samples. Feature manifold regularization improves the model's ability to learn complex patterns within the fuzzy feature space, thereby effectively utilizing the intrinsic correlations among features. As a semi-supervised learning approach, this method not only enhances the feature representation from a limited number of labeled samples but also leverages the similarities among samples, including those unlabeled samples, and the correlations within the fuzzy feature space, thereby further improving the model's predictive performance. Our proposed method has been applied to predict ICU utilization in recipients infected with COVID-19 post-transplantation, and the experimental results demonstrated its effectiveness compared to other algorithms.

# 2 THE PROPOSED METHODOLOGY

The architecture of the proposed D-DMR-FBLS system is depicted in Figure 1. The training process is methodically divided into two distinct phases. The initial phase, known as the Unsupervised Training Phase (UTP), focuses on feature representations from the input data through DBN and TSK fuzzy systems. The aim is to augment the feature representation capabilities of the FBLS. During this phase, the DBN and TSK fuzzy systems extract latent feature relationships and structure information within the input data. Following this, the second phase utilizes the feature representations derived from the first phase as inputs to the subsystems of the FBLS. Here, a series of nonlinear transformations are applied to compute the outputs of the enhancement nodes. An innovation in this phase is the introduction of a graph-based dual manifold regularization strategy, designed to not only unearth intrinsic relationships and correlations within the fuzzy feature space but also to bolster the system's ability in learning from unlabeled samples. Termed the Supervised Training Phase (STP), this stage involves training the system's parameters under supervision to determine the output layer's weights.

## 2.1 Neural Representation Based on Deep Belief Networks

During the UTP phase, we integrated a neural representation based on DBN to enhance the representation learning capability of FBLS. A DBN consists of multiple layers of stacked Restricted Boltzmann Machines (RBM). The input layer nodes correspond to the dimensionality of the input space, with $d$ features in the dataset. The hidden layers form the complete DBN neural representation. Assuming the DBN has $l$ hidden layers, the topmost layer nodes are $h_l = [h_{l1}, h_{l2}, \ldots, h_{ll}]$, and the layer below has nodes $h_{l-1}$. This hierarchical structure abstracts high-level features, progressively reducing or eliminating noise in the data.

The DBN pre-training starts with the first RBM, where the visible layer contains $d$ nodes represented by $v_1 = x$, and the first hidden layer nodes are $h_1 = [h_{11}, h_{12}, \ldots, h_{1n_1}]$. Unlike conventional DBNs requiring supervised fine-tuning, our model utilizes only the unsupervised pre-training stage to acquire neu-

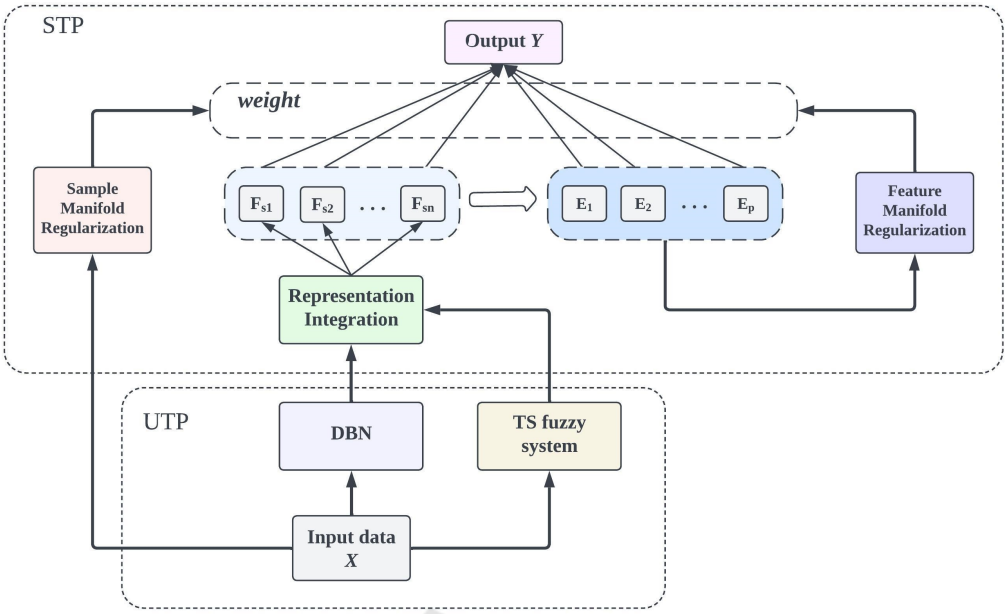


Figure 1: The structure of the proposed D-DMR-FBLS.

ral representations for each hidden layer. The Contrastive Divergence (CD) algorithm determines the weight matrix $W_k$, visible layer biases $b_k$, and hidden layer biases $c_k$ between the layers of each RBM.

For computational convenience, $h_{kj}$ and $v^r_{ki}$ are set to 1 if their probabilities exceed a random threshold, otherwise set to 0. The sigmoid function is defined as Eq. (1).

$$\mathrm{sigm}(x) = \frac{1}{1+e^{-x}} \tag{1}$$

The update formulas for weights $w_k$, biases $b_k$, and $c_k$ during the $t$-th iteration are defined as Eq. (2):

$$\begin{aligned} W_k^{(t)} =& W_k^{(t-1)} + \varepsilon \left( P\left(h_k^{(t-1)} \mid v_k^{(t-1)}\right)\left(v_k^{(t-1)}\right)^T \right. \\ & \left. - P\left(h_k^{r(t-1)} \mid v_k^{r(t-1)}\right)\left(v_k^{r(t-1)}\right)^T \right) \\ b_k^{(t)} =& b_k^{(t-1)} + \varepsilon\left(v_k^{(t-1)} - v_k^{r(t-1)}\right) \\ c_k^{(t)} =& c_k^{(t-1)} + \varepsilon\left(P\left(h_k^{(t-1)} \mid v_k^{(t-1)}\right)\right. \\ & \left. - P\left(h_k^{r(t-1)} \mid v_k^{r(t-1)}\right)\right) \end{aligned} \tag{2}$$

After pre-training each RBM, the first hidden layer output $h_1$ becomes the visible layer input for the next RBM, repeating this process sequentially for all RBMs. Once training is complete, the DBN parameters ($W_k$, $b_k$, and $c_k$) are fixed. Given an input vector $x = [x_1, x_2, \ldots, x_d]$, the nodes in the $k$-th hidden layer $h_k = [h_{k1}, h_{k2}, \ldots, h_{kk}]$ are calculated by Eq.( 3).

$$h_{kj} = \mathrm{sigm}\left(\sum_{i=1}^{n_k} W_{kij} v_{ki} + c_{kj}\right) \tag{3}$$

In the top hidden layer, the feature representation $[h_{l1}, h_{l2}, \ldots, h_{ll}]$ is integrated with the TSK fuzzy system output to form a neural fuzzy system. This system leverages the DBN's data representation capabilities to capture complex features while enhancing the model's understanding and capability to address complex data structures.

## 2.2 Fuzzy Representation Based on TSK Fuzzy System

FBLS comprises $n$ fuzzy subsystems and $p$ enhancement node groups. It accepts input data denoted as $X = (x_1, x_2, \ldots, x_N)^{\mathrm{T}}$ within $\mathbb{R}^{N\times M}$, where each sample feature is represented as $x_s = (x_{s1}, x_{s2}, \ldots, x_{sM}), s = 1, 2, \ldots, M$. Each fuzzy subsystem contains a set of fuzzy rules designed to extract features from the input data. For the $i$-th fuzzy subsystem with $k^i$ fuzzy rules, a series of first-order TSK fuzzy system rules are defined based on the input features, which can be expressed as:

$$z^i_{sk} = f^i_k(x_{s1}, x_{s2}, \ldots, x_{sM}) = \sum_{t=1}^{M} \alpha^i_{kt} x_{st} \tag{4}$$

where $k = 1, 2, \ldots, k^i$ is the fuzzy rule of the $i$-th fuzzy subsystem, $\alpha^i_{kt}$ is a coefficient uniformly distributed on the interval $[0, 1]$. In this study, for the $i$-th fuzzy subsystem, the training data is segmented into $k^i$ clusters, represented by $c_k$, utilizing the FCM method.

The FCM clustering method is used to minimize the objective function:

$$J_f(U,C) = \sum_{s=1}^{N}\sum_{k=1}^{k^i} u_{sk}^f \|x_s - c_k\|_2^2 \tag{5}$$

In Eq. (5), $m$ represents a fuzzification coefficient, $U = (u_{sk})_{N\times k^i}$ is a membership matrix, $u_{sk}$ indicates the degree of membership of $x_s$ in cluster $k$, and $c_k$ is the centroid of cluster $k$ in $M$-dimensional space. The optimization of the objective function $J_f(U,C)$ can be solved by iteratively updating the membership $u_{sk}$ and the centroid $c_k$, following these formulas:

$$u_{sk} = \left(\sum_{t=1}^{k^i}\left(\frac{\|x_s - c_k\|}{\|x_s - c_t\|}\right)^{\frac{2}{m-1}}\right)^{-1} \tag{6}$$

$$c_k = \sum_{s=1}^{N} u_{sk}^f \cdot x_s / \sum_{s=1}^{N} u_{sk}^f \tag{7}$$

Distinct from the k-means method, in the fuzzy C-means approach, the weighted firing strength in the $i$-th fuzzy subsystem is set as $w_{sk}^i = u_{sk}$. This eliminates the need for defining additional membership functions for the fuzzy rules. The intermediate output vector of the $i$-th fuzzy subsystem $Z_{si}$ is given by:

$$Z_{si} = \left(w_{s1}^i z_{s1}^i, w_{s2}^i z_{s2}^i, \ldots, w_{sk^i}^i z_{sk^i}^i\right) \tag{8}$$

## 2.3 DBN-Based Fuzzy Broad Learning System

Integrating the top hidden layer feature vectors of DBN with the output vectors of the TSK fuzzy system, we consider the feature representation vector of DBN, $[h_{l1}, h_{l2}, \ldots, h_{ll}]$, as well as the system output vector of the TSK Fuzzy System, $Z_{si}$. Given the dimensionality of the DBN's top hidden layer feature vector as $n_l$, and the output of each TSK Fuzzy subsystem based on $k^i$ fuzzy rules, we construct a combined feature representation vector, $Z_c$, shown as Eq. (9).

$$Z_c = [h_{l1}, h_{l2}, \ldots, h_{ll}, Z_{s1}, Z_{s2}, \ldots, Z_{sn}] \tag{9}$$

where $Z_c \in \mathbb{R}^{N\times\left(n_l + \Sigma_{i=1}^{n} k^i\right)}$. Here, $Z_{s1}, Z_{s2}, \ldots, Z_{sn}$ represent the output vectors from each subsystem of the TSK Fuzzy System, and $h_{l1}, h_{l2}, \ldots, h_{ll}$ represent the feature representation vector from the top hidden layer of the DBN.

Utilizing $Z_c$, this method employs nonlinear transformations in the enhancement layer (comprising $p$ groups of enhancement nodes) to obtain the output of the enhancement layer, $H^p$. This is defined as Eq. (10).

$$H^p = (H_1, H_2, \ldots, H_p) \in \mathbb{R}^{N\times\left(E_1+E_2+\ldots+E_p\right)} \tag{10}$$

Herein, $H_j (j = 1,2,\ldots,p)$ is computed as:

$$H_j = \varphi_j (Z_c W_j + \beta_j) \in \mathbb{R}^{N\times E_j} \tag{11}$$

Here, $E_j$ denotes the number of neurons in the $j$-th group of enhancement nodes. $W_j$ and $\beta_j$ are respectively the weights and biases for the intermediate output $Z_c$ from the fuzzy subsystems to the enhancement layer, which are randomly distributed within the range of $[0,1]$. $\varphi(\cdot)$ represents a type of nonlinear transformation.

$$\begin{aligned} Y &= [Z_c \mid H^p] \begin{bmatrix} W_c \\ W^h \end{bmatrix} \\ &= AW \end{aligned} \tag{12}$$

Here, $W_c$ is the weight matrix for the combined feature representation matrix $Z_c$ to the output layer. $W^h$ is the mapping matrix for the enhancement layer. $W$ is the weight matrix connecting all fuzzy subsystems and enhancement node layers to the output layer, calculated based on the system's output. According to (Cao et al., 2017), $W$ can be derived as:

$$W = \left(\lambda I + AA^{\mathrm{T}}\right)^{-1} A^{\mathrm{T}} Y \tag{13}$$

## 2.4 Dual Manifold Regularization Framework

In this study, DMR-FBLS incorporates dual manifold regularization mechanisms: sample-based and feature-based manifold learning. Sample-based manifold learning preserves the distributional characteristics of samples in the original space, ensuring that proximity in the original sample space is maintained in the lower-dimensional projected space. Feature-based manifold regularization hypothesizes that similar feature dimensions in the fuzzy feature space should have similar corresponding weights, filtering out noise and redundant features, thereby improving learning efficiency and generalization capability. This dual strategy effectively utilizes the internal structure of samples and the relations between fuzzy features, enhancing learning performance, especially in datasets with substantial unlabeled data.

### 2.4.1 Sample Manifold Regularization

If two samples are proximate in the input space, their outputs should be proximate in the target space. We use a Gaussian kernel function to measure the distance between samples:

$$s(\mathbf{x}_i, \mathbf{x}_j) = \exp\left(-\frac{\left\|\mathbf{x}_i - \mathbf{x}_j\right\|_2^2}{2\sigma_s^2}\right) \tag{14}$$

Here, $\sigma_s$ controls the kernel spread, affecting distance measurement. The similarity matrix $S$ is constructed, treating samples as nodes and their similarities as edges, forming an adjacency graph. The regularization term is defined as:

$$R_s(\mathbf{w}) = \frac{1}{2}\sum_{i,j=1}^{N} s_{ij}\left\|\mathbf{y}_i - \mathbf{y}_j\right\|_2^2 = \mathrm{tr}\left((AW)^T L_s (AW)\right) \tag{15}$$

Here, $L_s = H_s - S$ is the Laplacian matrix. This regularization strategy boosts the model's generalization performance by maintaining sample positions in the target space and capturing latent structural information in unlabeled data.

#### 2.4.2 Feature Manifold Regularization

The FBLS framework may result in a high-dimensional feature matrix with redundant features. Inspired by sample-based manifold regularization, we introduce feature-based manifold learning to reduce redundant feature influence. We hypothesize that correlated feature dimensions in the fuzzy feature space will have similar weight coefficients. The Gaussian kernel function quantifies the correlation between feature dimensions:

$$f\left(A^q, A^t\right) = \exp\left(-\frac{\|A^q - A^t\|_2^2}{2\sigma_f^2}\right) \tag{16}$$

The manifold regularization term is defined as:

$$\begin{aligned} R_f(W) &= \frac{1}{2}\sum_{q,t=1}^{N\times\left(C+E_1+E_2+\ldots+E_p\right)} f_{qt}\left\|W_q - W_t\right\|_2^2 \\ &= \mathrm{tr}\left(W^T L_f W\right) \end{aligned} \tag{17}$$

Here, $L_f = H_f - F$ is the Laplacian matrix. This approach effectively captures structural information in the fuzzy feature space.

### 2.5 Semi-Supervised DMR-FBLS

The objective function of the original FBLS fuzzy system is redefined as:

$$\begin{aligned} \min_W D\|y - AW\|_2^2 + \alpha\|W\|_2^2 \\ + \beta\,\mathrm{tr}\left((AW)^T L_s (AW)\right) \\ + \lambda\,\mathrm{tr}\left(W^T L_f W\right) \end{aligned} \tag{18}$$

By differentiating and setting the derivative to zero, we obtain:

$$A^T QAW + \alpha W + \beta A^T L_s AW + \lambda L_f W = A^T Qy \tag{19}$$

$W$ can be directly derived from the (19) as:

$$W = \left(A^T QA + \alpha I + \beta A^T L_s A + \lambda L_f\right)^{-1} A^T Qy \tag{20}$$

In semi-supervised learning, our framework integrates both labeled and unlabeled data. The labeled dataset is encapsulated as $\{X_l, y_l\} = \{x_i, y_i\}_{i=1}^{l}$, where $l$ denotes the count of labeled instances. Conversely, the unlabeled dataset is denoted as $X_u = \{x_j\}_{j=1}^{u}$, with $u$ symbolizing the number of unlabeled samples. In (20), $\alpha$, $\beta$, $\lambda$ are coefficients corresponding to the regularization term, the sample manifold regularization, and the feature manifold regularization, respectively. The weight matrix $Q$, a diagonal matrix, plays a role in filtering and weighting the samples. In this study, for the diagonal matrix $Q$, the diagonal elements corresponding to the first l rows and columns, which represent the labeled data, are set to 1. The remaining diagonal elements are set to 0. The Laplace matrices $L_s$ and $L_f$ are computed based on similarity measures derived from both labeled and unlabeled data. This design efficiently exploits the structural information and feature relationships inherent in the unlabeled data.

## 3 EXPERIMENTAL SETUP

In this section, we will provide a detailed description of the dataset utilized in this experiment, as well as the classifiers and evaluation metrics employed.

### 3.1 Dataset

The IDOTCOVID database represents a comprehensive global resource, encompassing data from approximately 1200 patients across 78 transplant centers in 11 different countries, collected between March 2020 and March 2021. This database incorporates a wide array of variables, including demographic and transplant-related information, as well as epidemiological, clinical manifestations, and treatment management of solid organ transplant (SOT) patients during the COVID-19 pandemic. The descriptive statistics for the IDOTCOVID database are shown in Table. 1.

### 3.2 Classifiers and Evaluation Metrics

To evaluate the DMR-FBLS model's performance and compare it with other mainstream algorithms, we selected eight distinct ML models. These models, including XGBoost, RF, and AdaBoost, represent various ML categories and have been validated in their domains, particularly in organ transplantation research for their accuracy and robustness (Zhang

Table 1: Descriptive Statistics for IDOTCOVID database.

| Data | Statistics results |
|---|---|
| Recipients | 1267 |
| Average Age | 56.17 |
| Gender | Female (448), Male (819) |
| Average Age at SOT | 47.39 |
| Total Attribute | 206 |
| SOT Type | Kidney: 64.88%, Liver: 33.46% |
| Patient Country | Spain (908), Mexico (211), Argetina (147), Italy (69), etc. |
| Demographic Attributes | Age, Gender, Country, DOB, Age at SOT, etc. |
| Clinical Attributes | Type of SOT, Diagnosis, Symptoms, Manifestations, etc. |
| Treatment Attributes | Kaletra, Remdesivir, CsA-Red, etc. |
| Admission Attributes | Blood Pressure, Vasoactive drugs, X-ray, etc. |
| Categories of Attributes | Various (incl. Demographics, Clinical, Treatment, Admission) |

et al., 2022; Liu et al., 2020). Decision Trees (DT) are known for their interpretability and efficiency with categorical data, essential in clinical decision-making. BLS and Multi-Layer Perceptron (MLP) represent neural networks with strong function mapping capabilities. FBLS and TSK are fuzzy systems that handle uncertainty well, showing good performance in multiple studies (Peng and ChunHao, 2022; Xue et al., 2018). This diverse selection ensures a thorough assessment of D-DMR-FBLS across different scenarios. We split each dataset into 70% training and 30% testing sets, optimized hyperparameters using five-fold cross-validation on the training set, and executed each algorithm 50 times. Performance was evaluated using four key metrics: accuracy, AUC, F1-score, and G-mean.

# 4 EXPERIMENTAL RESULT AND DISCUSSION

## 4.1 Comparative Results and Analysis

The results in Table 2 compare the performance of various models predicting ICU admission among COVID-19 infected organ transplant recipients. The D-DMR-FBLS model excelled across all metrics, achieving an accuracy of 0.899, AUC of 0.853, G-mean of 0.727, and F1-score of 0.666, outperforming other models. This confirms D-DMR-FBLS's superior accuracy and balanced classification efficiency.

The mainstream ML algorithms like XGBoost, RF, and Adaboost performed well in AUC but poorly in G-mean and F1-score, crucial for handling class imbalance. The FBLS model outperformed the BLS model across all metrics, showing its capability in processing complex data. Integrating the TSK fuzzy subsystem into BLS improved its recognition of minority class samples.

Figure 2 shows the performance of four BLS-based algorithms across four metrics. Ablation experiments highlight D-DMR-FBLS's superior performance, especially in G-mean and F1-score. The

Table 2: The performance comparison for different models on ICU admission prediction.

| Method | Accuracy | AUC | G-mean | F1-score |
|---|---|---|---|---|
| D-DMR-FBLS | **0.899** | **0.853** | **0.727** | **0.666** |
| FBLS | 0.890 | 0.833 | 0.706 | 0.618 |
| BLS | 0.867 | 0.815 | 0.678 | 0.579 |
| TSK | 0.875 | 0.823 | 0.702 | 0.611 |
| XGBoost | 0.862 | 0.837 | 0.629 | 0.518 |
| RF | 0.861 | 0.842 | 0.516 | 0.400 |
| MLP | 0.856 | 0.824 | 0.687 | 0.506 |
| Adaboost | 0.868 | 0.839 | 0.569 | 0.475 |
| DT | 0.846 | 0.790 | 0.601 | 0.468 |

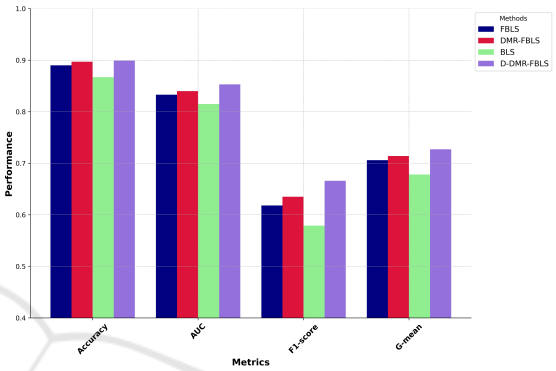


Figure 2: Comparative results of ablation experiments across various metrics for D-DMR-FBLS, DMR-FBLS, FBLS, and BLS.

Table 3: Results of the Wilcoxon signed-rank test, with D-DMR-FBLS serving as the control algorithm. If the p-value for a particular method is less than 0.05, it indicates a significant performance difference between that method and D-DMR-FBLS.

| | Accuracy | AUC | F-score | G-mean |
|---|---|---|---|---|
| FBLS | **0.0409** | **0.0000** | **0.0000** | **0.0012** |
| DMR-FBLS | 0.8333 | **0.0106** | **0.0037** | 0.0991 |
| BLS | **0.0000** | **0.0000** | **0.0000** | **0.0001** |
| TSK | **0.0002** | **0.0000** | **0.0000** | **0.0040** |
| XGBoost | **0.0000** | **0.0048** | **0.0000** | **0.0000** |
| RF | **0.0000** | **0.0056** | **0.0026** | **0.0000** |
| MLP | **0.0000** | **0.0000** | **0.0000** | **0.0001** |
| Adaboost | **0.0000** | **0.0027** | **0.0012** | **0.0000** |
| DT | **0.0000** | **0.0000** | **0.0000** | **0.0000** |

FBLS model showed performance improvements over BLS. Adding graph manifold regularization (feature-based and sample-based) to DMR-FBLS further enhanced performance by uncovering the correlation within feature space and hidden data structure. Incorporating DBN into DMR-FBLS to form D-DMR-FBLS improved all metrics. DBN deepens the model's representation learning, capturing hidden data characteristics and boosting classification performance when combined with the TSK fuzzy system.

Table 3 uses the Wilcoxon signed-rank test to compare D-DMR-FBLS against other algorithms.

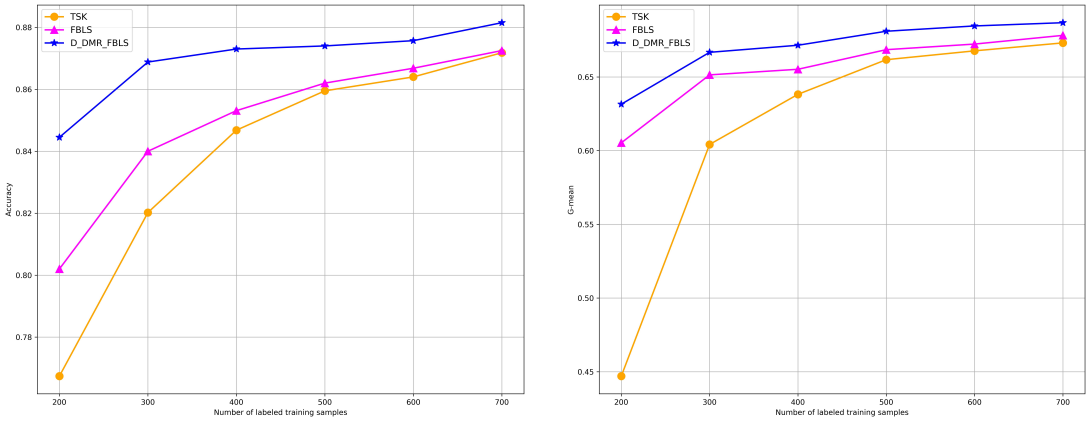


(a) Accuracy comparison.

(b) G-Mean Comparison.

Figure 3: Performance of accuracy with unlabeled training samples and varying quantities of labeled training samples.

Except for DMR-FBLS, which showed no significant difference in accuracy and G-mean (p-values $> 0.05$), most other algorithms had p-values $< 0.05$, indicating significant differences and rejecting the null hypothesis. This demonstrates D-DMR-FBLS's substantial performance advantage.

## 4.2 Comparative Experiment on Using Unlabeled and Limited Labeled Samples

To evaluate our proposed algorithm with limited labeled and unlabeled samples, we compared it with other fuzzy systems. From the original ICU admission dataset, we extracted 567 samples and concealed their labels to create an unlabeled dataset. We then stratified samples according to label categories and selected 200, 300, 400, 500, 600, and 700 labeled samples to test the model's performance with varying labeled data. This approach assesses the applicability and performance of the proposed algorithms in a weakly-supervised learning context.

In this experiment, we evaluated and compared the performance of three fuzzy systems—D-DMR-FBLS, FBLS, and TSK—using unlabeled samples and a varying number of labeled samples. Through this experiment, we aim to evaluate the performance of different fuzzy systems in scenarios with small sample sizes and lacking labeled samples. As can be seen from Figure. 3a and Figure. 3b, at fewer labeled sample sizes (200 and 300 samples), the result reveals that the accuracy of the D-DMR-FBLS model considerably surpasses that of FBLS and TSK fuzzy models, indicating D-DMR-FBLS's effective learning capability and strong generalization ability with limited label. As the number of labeled samples increases to a relatively higher range (from 500 to 700 samples), the improvement in accuracy and G-mean values for all three models starts to stabilize. Within this sample size bracket, the DMR-FBLS model maintain the highest accuracy, yet the performance gap between the TSK and FBLS models begins to narrow. In general, the trend suggests that when faced with a small number of labeled samples and the presence of unlabeled samples, the D-DMR-FBLS model demonstrates a significant advantage over the other two fuzzy systems. However, while the performance of all models improves with an increase in the number of labeled samples, the rate of improvement decelerates, indicating that additional labeled information has a limited impact on enhancing model performance beyond a certain sample volume threshold. Overall, from the experimental results, we can conclude that the D-DMR-FBLS model demonstrates strong learning capabilities and robust generalization abilities compared to the other fuzzy systems under the scenario with a small number of labeled and unlabeled samples.

# 5 CONCLUSION

This study introduces a novel semi-supervised Dual-Manifold Regularized Fuzzy Broad Learning System (D-DMR-FBLS), aimed at enhancing the predictive performance for ICU admissions among post-COVID organ transplant recipients. Our method enhances the representation learning capability through the use of DBN and TSK fuzzy systems in the UTP phase, thereby enriching the model's capacity to process and learn from complex data structures. Besides, our approach integrates feature manifold regularization and sample manifold regularization with FBLS, improv-

ing the model's generalization capability. According to experimental results, the D-DMR-FBLS outperformed other models in terms of accuracy, AUC, F1-score and G-mean. Besides, its performance surpasses the FBLS and TSK fuzzy systems, especially in scenarios with limited labeled samples. This new neuro-fuzzy system shows promise for use in contexts with limited medical resources, assisting the decision-making for the allocation of medical care to organ transplant recipients. Future research could further explore the application of D-DMR-FBLS across other medical datasets, validating its effectiveness in varied medical contexts.

## ACKNOWLEDGEMENTS

This paper is part of project PID2022-143299OB-I00, financed by MCIN/AEI/10.13030/501100011033/FEDER,UE.

## REFERENCES

Cao, B., Mao, M., Viidu, S., and Philip, S. Y. (2017). Hitfraud: a broad learning approach for collective fraud detection in heterogeneous information networks. In *2017 IEEE international conference on data mining (ICDM)*, pages 769–774. IEEE.

Ershoff, B. D., Lee, C. K., Wray, C. L., Agopian, V. G., Urban, G., Baldi, P., and Cannesson, M. (2020). Training and validation of deep neural networks for the prediction of 90-day post-liver transplant mortality using unos registry data. In *Transplantation proceedings*, volume 52, pages 246–258. Elsevier.

Feng, S. and Chen, C. P. (2018). Fuzzy broad learning system: A novel neuro-fuzzy model for regression and classification. *IEEE transactions on cybernetics*, 50(2):414–424.

Feng, S. and Chen, C. P. (2021). Performance analysis of fuzzy bls using different cluster methods for classification. *Science China Information Sciences*, 64:1–3.

Feng, S., Chen, C. P., Xu, L., and Liu, Z. (2020). On the accuracy–complexity tradeoff of fuzzy broad learning system. *IEEE Transactions on Fuzzy Systems*, 29(10):2963–2974.

Gong, X., Zhang, T., Chen, C. P., and Liu, Z. (2021). Research review for broad learning system: Algorithms, theory, and applications. *IEEE Transactions on Cybernetics*, 52(9):8922–8950.

Liu, C.-L., Soong, R.-S., Lee, W.-C., Jiang, G.-W., and Lin, Y.-C. (2020). predicting short-term survival after liver transplantation using machine learning. *Scientific reports*, 10(1):1–10.

Liu, Z., Huang, S., Jin, W., and Mu, Y. (2021). Broad learning system for semi-supervised learning. *Neurocomputing*, 444:38–47.

Mamode, N., Ahmed, Z., Jones, G., Banga, N., Motallebzadeh, R., Tolley, H., Marks, S., Stojanovic, J., Khurram, M. A., Thuraisingham, R., et al. (2021). Mortality rates in transplant recipients and transplantation candidates in a high-prevalence covid-19 environment. *Transplantation*, 105(1):212–215.

Mark, E., Goldsman, D., Gurbaxani, B., Keskinocak, P., and Sokol, J. (2023). Predicting a kidney transplant patient's pre-transplant functional status based on information from waitlist registration. *Scientific Reports*, 13(1):6164.

Peng, C. and ChunHao, D. (2022). Monitoring multidomain batch process state based on fuzzy broad learning system. *Expert Systems with Applications*, 187:115851.

Shihabudheen, K. and Pillai, G. N. (2018). Recent advances in neuro-fuzzy system: A survey. *Knowledge-Based Systems*, 152:136–162.

Worldometer (2024). Worldometer - COVID-19 Coronavirus Pandemic. https://www.worldometers.info/coronavirus/. Accessed: 2024-01-10.

Xue, J., Jiang, Y., Wang, L., Sun, Z., and Xing, C. (2018). Intelligent prediction of renal injury in diabetic kidney disease patients based on a novel unbalanced zero-order tsk fuzzy system. *Journal of Medical Imaging and Health Informatics*, 8(8):1711–1717.

Zhang, L., Li, J., Lu, G., Shen, P., Bennamoun, M., Shah, S. A. A., Miao, Q., Zhu, G., Li, P., and Lu, X. (2020). Analysis and variants of broad learning system. *IEEE Transactions on Systems, Man, and Cybernetics: Systems*, 52(1):334–344.

Zhang, X., Gavaldà, R., and Baixeries, J. (2022). Interpretable prediction of mortality in liver transplant recipients based on machine learning. *Computers in biology and medicine*, 151:106188.